Analysis of flow and aerodynamic noise behaviour of a simplified high-speed train bogie inside the bogie cavity

J. Y. Zhu[1], Z. W. Hu[1], D. J. Thompson[2]

[1] Aerodynamics and Flight Mechanics Research Group, Faculty of Engineering and the Environment, University of Southampton, Southampton SO17 1BJ, United Kingdom
[2] Institute of Sound and Vibration Research, Faculty of Engineering and the Environment, University of Southampton, Southampton SO17 1BJ, United Kingdom

Abstract: Aerodynamic noise becomes significant for high-speed trains but its prediction in an industrial context is difficult. The flow and aerodynamic noise behaviour of a simplified high-speed train bogie at scale 1:10 are studied here through numerical simulations. The bogie is situated in the bogie cavity and cases without and with a fairing are considered, allowing the shielding effect of the bogie fairing on sound generation and radiation to be investigated. A two-stage hybrid method combining computational fluid dynamics and acoustic analogy is applied. The near-field unsteady flow is obtained by solving the unsteady three-dimensional Navier-Stokes equations numerically using delayed detached-eddy simulation and the data are utilized to predict far-field noise signals based on the Ffowcs Williams-Hawkings acoustic analogy. Results show that when the bogie is located inside the bogie cavity, the shear layer developed from the cavity leading edge interacts strongly with the flow separated from the bogie upstream components and the cavity wall. Therefore, a highly turbulent flow is generated within the bogie cavity due to flow impingement and recirculation within the cavity. It is found that, for noise calculated from the bogie surface sources of both cases, the directivity exhibits a lateral dipole pattern with dominant radiation in the axial direction. Compared with the no fairing case, the noise level is about 1 dB higher in the bogie symmetry plane along the axle mid-span for the fairing case where a stronger flow interaction is produced around the bogie central region. Moreover, the noise radiated to the trackside is predicted based on a permeable integration surface close to the bogie and parallel to the carbody side wall. The results show that the bogie fairing is effective in reducing the noise levels in most of the frequency range due to its shielding effect and a noise reduction around 3 dB is achieved for the current model case by mounting a fairing in the bogie area.

1. Introduction

For high-speed trains, it is generally accepted that the aerodynamic noise becomes predominant at running speeds over about 300 km/h [1-3]. Significant progress has been made in the understanding of the aerodynamic phenomena associated with high-speed trains [4,5]. In contrast, the generation of aerodynamic noise from high-speed trains is less well understood and numerical calculations have been restricted to some simple geometries using the traditional computational fluid dynamics methods [3]. The flow-induced noise from a full-scale simplified high-speed train was studied numerically using the lattice-Boltzmann method, although verification by experimental measurements is required to improve confidence [6,7]. By comparison, the calculations on some simplified scaled geometries can reveal more details of the flow behaviour and the corresponding aeroacoustic mechanisms in some main components of high-speed trains. Moreover, these numerical simulations can be performed with affordable computer resources and verified by experimental measurements. This paper aims to investigate the aerodynamic and aeroacoustic behaviour of the flow past a 1:10 scale simplified high-speed train bogie located inside the bogie cavity and the effect of a fairing on the noise generation from the bogie region.

E-mail addresses:
jz1e10@soton.ac.uk (J. Y. Zhu), z.hu@soton.ac.uk (Z. W. Hu), djt@isvr.soton.ac.uk (D. J. Thompson)

2. Numerical Method

Numerical simulations are carried out using a two-stage strategy of computational fluid dynamics and computational aeroacoustics methods. Aerodynamically, high-speed trains are operating within the low Mach number flow regime. The incoming flow simulated here is at a low Mach number of 0.09 (corresponding to 30 m/s) and thereby the compressibility effects may be neglected compared with the hydrodynamic flow field. Therefore, the unsteady, incompressible Navier-Stokes equations are used to solve the flow field. The open source software OpenFOAM-2.2.1 is employed for the current flow simulations. A scheme of second-order accuracy is used for the spatial derivatives and the temporal discretization follows a second-order fully implicit scheme. The delayed detached-eddy simulation (DDES) based on the Spalart-Allmaras turbulence model is applied for the flow calculations [8]. The near-field unsteady flow computation provides acoustic sources, which are applied in the Ffowcs Williams-Hawkings (FW-H) acoustic analogy for far-field noise prediction [9].

3. Simulation Setup

Fig. 1 shows the models of the simplified bogie inside the bogie cavity without and with fairing used in this study. These represent a simplified bogie geometry at 1:10 scale. The axle has a diameter (d) of 17.5 mm and the wheels have a diameter (D) of 92 mm. The centre-to-centre spacing of the two axles is 252 mm, which is 14 times the axle diameter. The carbody under-floor surfaces are level with the bogie horizontal central plane. The fairing is shown in Fig. 1(b). It has a thickness of 3.5 mm and an identical length and depth to the bogie cavity. The top half of the bogie is situated within the bogie cavity and covered by the fairing.

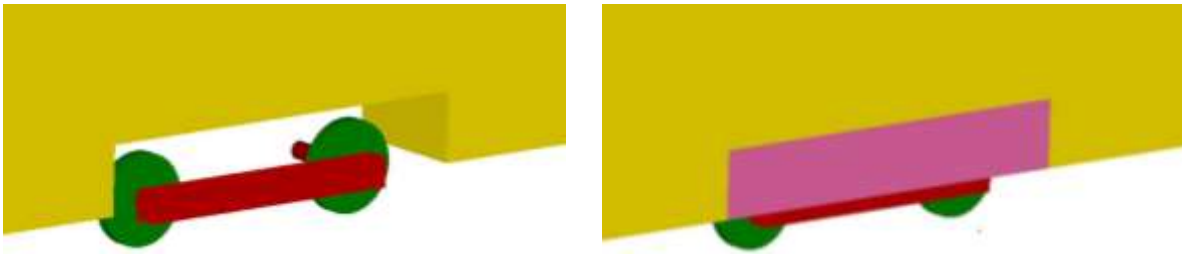

(a) Without fairing (b) With fairing

Fig. 1. Models of a simplified bogie inside the cavity

These bogie-inside-cavity cases are symmetrical about the axle mid-span where the influence from the three-dimensional flow from the wheel and frame is small; therefore it is reasonable to include only half of the geometry and make use of the symmetry to reduce the computational cost. The computational domain has dimensions of $20.7D$, $11D$ and $6.3D$ (where D is the wheel diameter) along the streamwise (x), vertical (y) and spanwise (z) directions, respectively. Thus, the outlet and side boundaries are far enough away to have negligible influence on the flow developed around the bogie and the cavity.

A fully structured mesh is generated around all geometries. The distance from the bogie, cavity wall and fairing surfaces to the nearest grid point is set as 10^{-5} m and stretched with a growth ratio of 1.1 inside the boundary layer, yielding a maximum value of y^+ (the dimensionless first-cell spacing) less than 1 to ensure the correct turbulence model is employed inside the viscous sublayer to account for the low-Reynolds number effects. The total number of grid points in the entire domain is 36.5 million for the bogie-inside-cavity case without fairing and 38.9 million for the case with fairing. The same mesh topology was employed for the isolated wheelset and bogie cases in which good agreement was achieved between numerical simulations and experimental measurements for the radiated far-field noise [10].

The boundary conditions applied are as follows: the upstream inlet flow is represented as a steady uniform flow (U_0=30 m/s) with a low turbulence intensity; the top, bottom, axle mid-plane and side boundaries are specified as having symmetry boundary conditions which are equivalent to zero-shear slip walls; a pressure outlet with zero gauge pressure is imposed at the downstream exit boundary and all solid surfaces are defined as stationary no-slip walls. Simulations are run with a physical time-step size of 10^{-5} s, which gives an adequate temporal resolution for the implicit time marching scheme used with a maximum Courant-Friedrichs-Lewy value of 2 within the computational domain.

4. Aerodynamic Results

In order to understand the flow-field characteristics developed around the geometries, the instantaneous iso-surfaces of Q criterion, the vorticity fields and the gauge pressure at wake positions are presented and compared.

4.1. Flow field

Fig. 2 visualizes the iso-surfaces of the second invariant of the velocity gradient Q to get an overview of the unsteady flow developed around the bogie in the bogie cavity without fairing. The second invariant of the velocity gradient Q is defined as $Q = \frac{1}{2}\left(\Omega_{ij}\Omega_{ij} - S_{ij}S_{ij}\right)$ in which $S_{ij} = \left(u_{i,j} + u_{j,i}\right)/2$ and $\Omega_{ij} = \left(u_{i,j} - u_{j,i}\right)/2$ are respectively the symmetric and antisymmetric components of velocity gradient. This identifies the vortical structures of the turbulent flow. Here the iso-surfaces are plotted at a normalized value of 50 (based on $Q/[(U_0/D)^2]$, where D is the wheel diameter). They are coloured by the velocity magnitude.

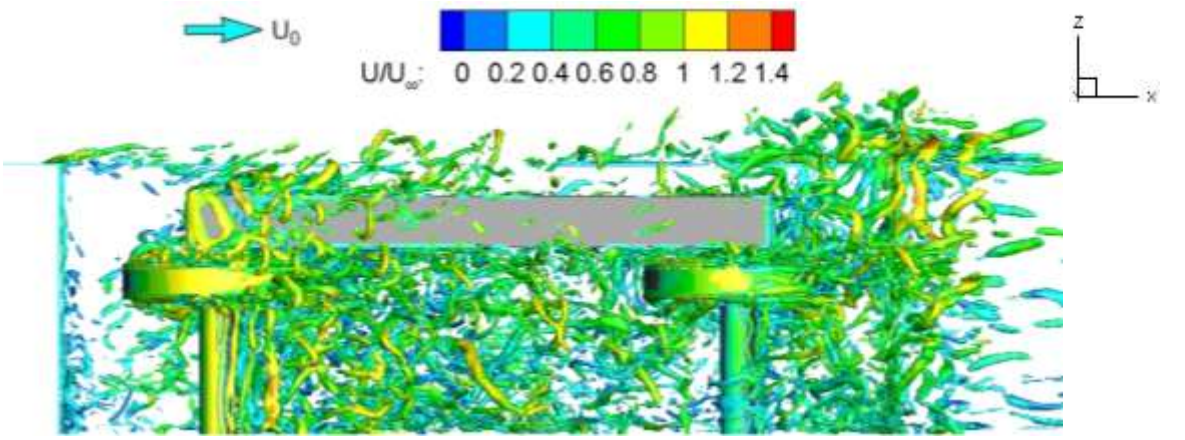

(a) Bottom view

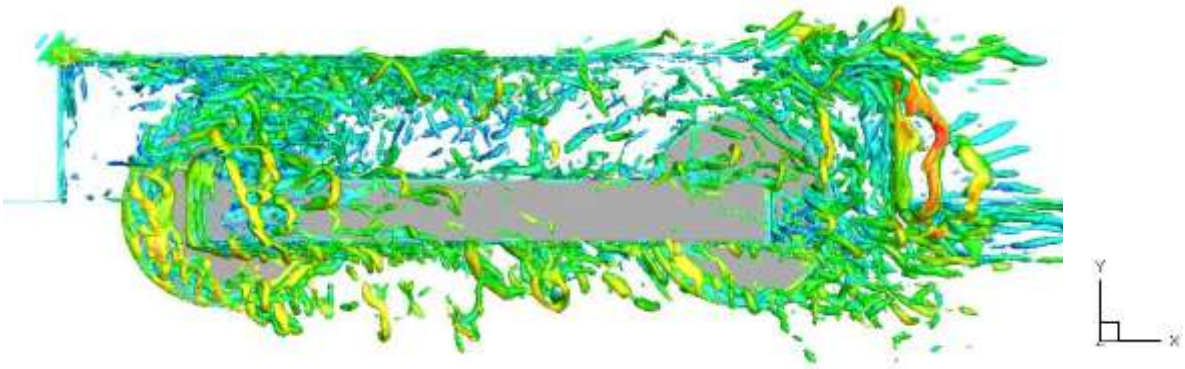

(b) Side view

Fig. 2. Iso-surfaces of the instantaneous normalized Q criterion coloured by the velocity magnitude (no fairing case)

Fig. 2(a) shows that the vortices shed from the upstream geometries impinge on the downstream ones, generating a highly turbulent wake behind the bogie. Subsequently, all vortices impinge on the cavity rear wall, deform largely and are merged into the eddies formed downstream behind the cavity. It can be observed from Fig. 2(b) that the different scales of vortices are generated between the upstream wheelset and cavity top wall as the various flow interactions and impingements occur there. Moreover, compared with the flow developed around the bogie, a higher level of flow-field unsteadiness is generated in the wake close to the cavity rear wall; nevertheless, it dissipates rapidly downstream as the flow development is impeded by the wall surface of the vehicle carbody.

Fig. 3(a) depicts contours of the instantaneous non-dimensional spanwise vorticity field ($\omega_Z = (\partial V/\partial x - \partial U/\partial y)D/U_\infty$, where D is the wheel diameter) in the axle mid-span for the case without fairing. It shows that a shear layer is shed from the cavity leading edge and bent upwards quickly in the streamwise direction. This shear layer travels downstream, turns towards the cavity and interacts with the flow separated from the upstream axle. Subsequently, all vortices are mixed up and impinge on the upper wall of the cavity, leading to the unsteady flow with complex structure formed there. Additionally, it can be observed that the wake behind both the upstream and downstream axles is highly turbulent. As the downstream axle is sufficiently far away from the upstream one, the vortex shedding may be generated from both axles as a co-shedding flow pattern. The downstream axle experiences the impingement of vortices shed from the upstream axle and the vortices developed behind the downstream axle are greatly deformed as they impinge on the cavity rear wall; thereby, all vortices are amalgamated behind the rear axle, leading to the downstream axle wake and the flow near the cavity rear corners becoming highly irregular and unsteady.

In comparison with the flow developed behind the axles, the flow around the wheels shows different characteristics, as displayed in Fig. 3(b) for the instantaneous spanwise vorticity field (ω_Z) contours in the wheel mid-span. The shear layer generated from the cavity leading edge is bent upwards and attached on the wheel tread as the gap between the wheel and cavity leading edge is relatively small. Subsequently, the vortices are separated from the wheel top surfaces as a consequence of the interaction between the attached shear layer and the boundary layer developed on the wheel tread. Note that the wake behind the upstream wheel is less organized and is three-dimensional. The incident vortices convected from the upstream wheel impinge on and interact with the vortices separated from the downstream wheel, resulting in a highly turbulent flow generated around the area of the downstream wheel and cavity rear wall as well as the corner.

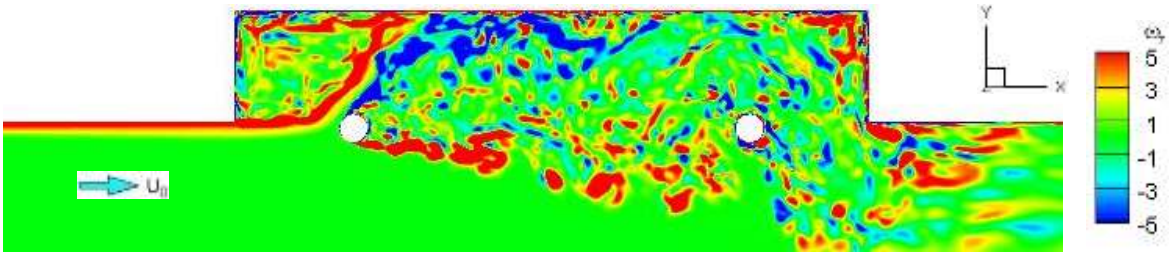

(a) Axle mid-span

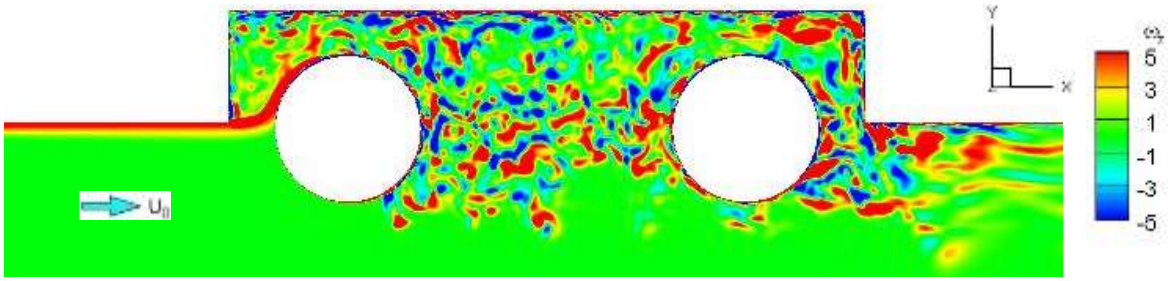

(b) Wheel mid-span

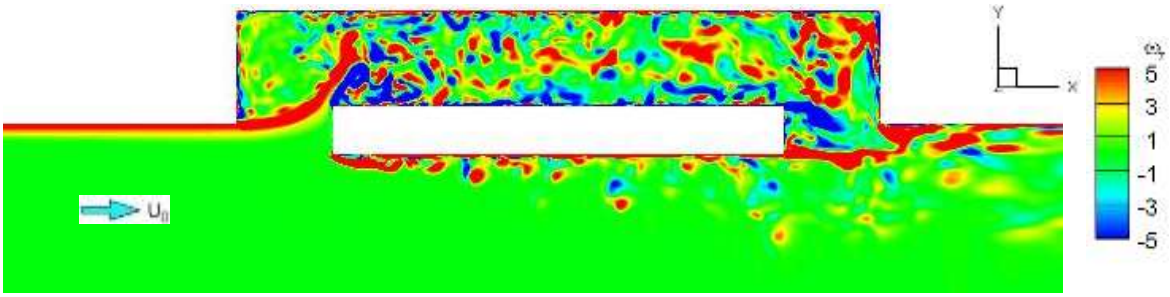

(c) Frame mid-span

Fig. 3. Contours of the instantaneous spanwise vorticity fields in a vertical plane for a bogie without fairing (side views)

The contour of the instantaneous spanwise vorticity field (ω_Z) along the frame mid-span is displayed in Fig. 3(c). Similarly, a shear layer developed from the cavity leading edge is bent upwards and interacts with the vortices separated from the frame top surfaces; thus, the vortical structure between the frame and the cavity top wall becomes highly turbulent due to flow impingement and recirculation occurring there. The vortices developed and convected along the frame surface are separated at the frame ends, generating an unsteady wake region between the frame and the cavity wall.

4.2. Wall pressure fluctuations

Fig. 4 displays the wall fluctuating pressure level in decibels ($L_p = 10\log(\overline{p'^2}/p_{ref}^2)$, where $\overline{p'^2}$ is mean-square fluctuating pressure and p_{ref} is reference acoustic pressure $20\mu Pa$) on the bogie surfaces for the bogie-inside-cavity cases without and with fairing, which can be used to identify the potentially significant noise source regions. It shows that for both cases, a high pressure fluctuation appears on the wheel and frame inner side surface and the axle surface near the axle-wheel junction region; and by comparison, the surface pressure fluctuations are considerably higher on these areas for the fairing case. This is due to the stronger flow impingement and interaction occurring around the bogie inside the cavity shielded by fairing, suggesting that more flow-induced noise may potentially be generated from the bogie structure itself.

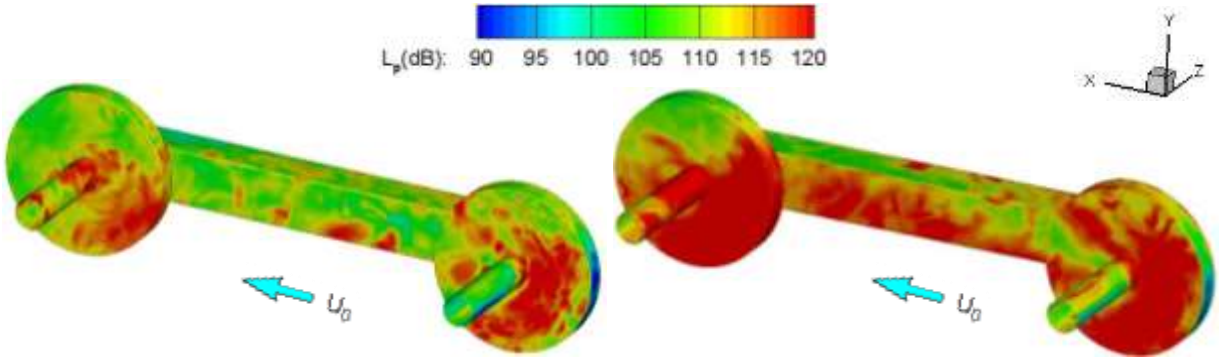

(a) Without fairing (b) With fairing

Fig. 4. Wall pressure fluctuation level of bogie surfaces inside the cavity

5. Aeroacoustic Results

When the transient flow field has become statistically steady, the far-field noise can be predicted by the FW-H method based on the near-field unsteady flow data. Firstly, noise assumed to be generated from the bogie solid surfaces alone is calculated and compared for the two cases in which the receivers are distributed uniformly with a resolution of 5° for the azimuthal and polar angles on a spherical surface with a radius of 2.5 m. Then, the FW-H method using permeable data surfaces is applied to predict the far-field noise including the shielding effect of the fairing on noise propagation. The permeable surface should be located far enough from the carbody side wall so that it is not influenced by the vortices which are mainly developed from the bogie cavity and convected in the downstream direction.

5.1. Noise directivity from bogie wall surfaces

The directivity of the radiated noise calculated in the far field is obtained based on the overall sound pressure level (OASPL). Assuming that the near-field wall pressure fluctuation on the bogie surfaces are radiated to free space, Fig. 5 displays the three-dimensional directivity pattern of the noise generated from the whole bogie surfaces to see the difference between the bogie-cavity cases without and with fairing. This is centred at the midpoint of the bogie and shows that the noise directivity of the bogie in the two cases exhibits a similar lateral dipole pattern with dominant radiation towards the trackside direction. The noise amplitudes are very similar in both cases except in the bogie symmetry plane along the axle mid-span where the noise level is about 1 dB higher for the fairing case as a consequence of the stronger flow interactions generated around the bogie central region. Note that the noise prediction here is different with the real case as the shielding effect from the bogie cavity wall and the fairing is not accounted. If a permeable data surface is applied for noise prediction using the acoustic analogy, all physical noise sources from all geometries can be enclosed in the surface

source terms and the acoustic propagation effect may be included in the noise radiation. For the current low Mach number flow, the noise contribution from the quadrupole source is small and may be neglected.

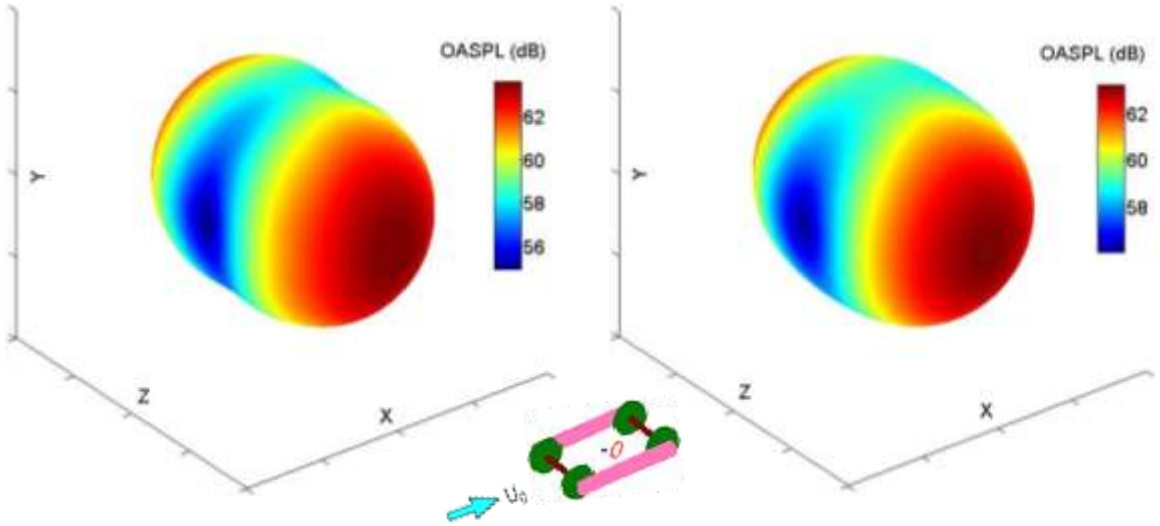

(a) Without fairing (b) With fairing

Fig. 5. Three-dimensional noise directivity radiated from bogie surfaces inside the cavity (centre of directivity pattern corresponds to 40 dB)

5.2. Noise spectra from permeable integration surfaces

As stated earlier, the noise generated from the bogie solid surfaces alone radiated to the trackside receivers is very similar in the cases without and with the fairing. Additionally, however, the noise generated inside the bogie cavity will be shielded by the fairing. Moreover, a certain amount of noise will be produced by the bogie cavity flow impinging on the cavity walls. Therefore the radiated noise is calculated using the acoustic analogy implemented on a permeable surface located at a distance of $0.3D$ (where D is the bogie cavity depth) from the car sidewall, extending over the whole height and length of the domain. This accounts for the noise generated from the wall pressure fluctuation and the turbulent flow around all the geometries including the bogie, bogie cavity and the carbody. Fig. 6 depicts the far-field noise spectra of the two cases based on the numerical simulations on the half bogie shown in Fig. 1. The trackside receiver is located 2.5 m away and 0.35 m above the bogie centre. It is found from Fig. 6(a) that the spectrum level is lower for the bogie cavity case with fairing in most of the frequency range below 2 kHz and the corresponding OASPL is 71.8 dB, about 3 dB lower than the case without fairing, the level of which is 74.7 dB. A broad hump between 30 Hz and 150 Hz is observed in the noise spectra of both cases and corresponds with the cavity flow interacting with the bogie. Note that since the sound speed is effectively infinite in an incompressible flow solver, the acoustic propagation and scattering will not be properly captured on the permeable surface. Thus, the noise reduction predicted could be slightly greater if the sound shielding effect from the bogie fairing were calculated by a compressible flow solver. Moreover, assuming that the noise is generated only from the bogie solid surfaces and radiated to the free space, the results are shown in Fig. 6(b) and the OASPL is around 60 dB for both bogie-inside-cavity cases. By comparison, the noise generated from the permeable integration surfaces is about 10-15 dB higher than that from the bogie solid surfaces alone. This is due to the pressure fluctuation around the surfaces of all geometries is calculated by the permeable surface, and therefore, the corresponding noise generation is larger.

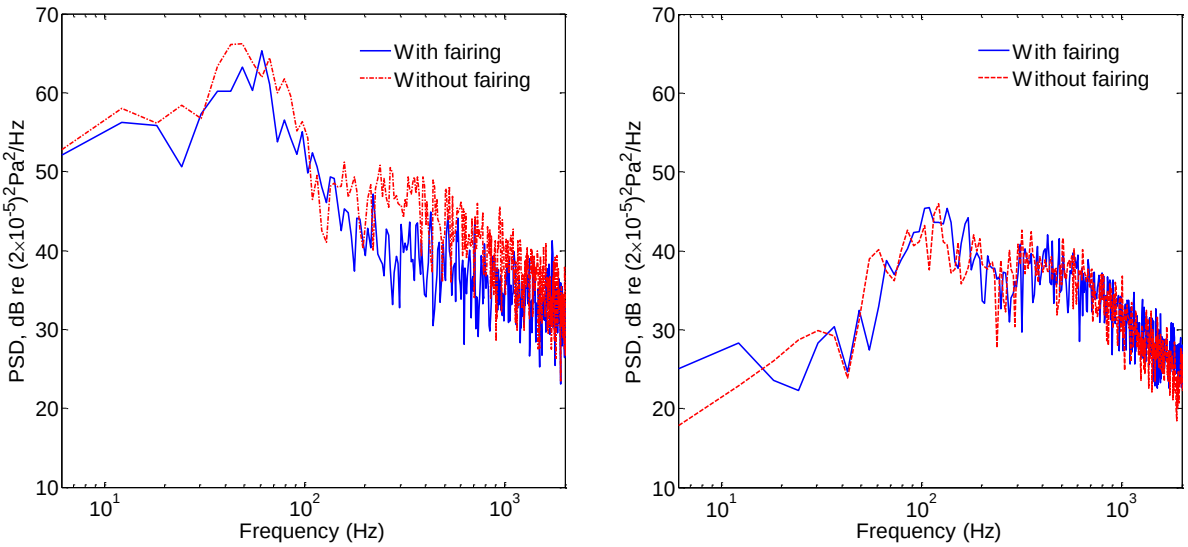

(a) Permeable surfaces (b) Bogie solid surfaces alone

Fig. 6. Comparisons of far-field noise spectra in bogie-inside-cavity cases

6. Conclusions

The flow behaviour and the aerodynamic noise characteristics developed from a scaled simplified bogie inside a bogie cavity without and with a fairing have been calculated using the DDES model and the FW-H acoustic analogy method. It is found that for the current bogie-inside-cavity cases, a shear layer developed from the cavity leading edge has a strong interaction with the flow separated from the bogie upstream components and the cavity wall. All vortices are mixed up and convected downstream and impinge on the downstream geometries and the cavity trailing edge. Thus, a highly irregular and unsteady flow is generated inside the bogie cavity due to the considerably strong flow interactions and recirculations occurring there. Moreover, for the comparison of the two cases, the noise generated from the bogie solid surfaces alone is assumed and predicted to have a lateral dipole pattern of sound radiation. The noise amplitudes are slightly higher in the bogie symmetry plane along the axle mid-span for the fairing case, suggesting interaction with the fairing increases surface noise sources. Noise generation from a permeable surface close to the bogie and parallel to the carbody side wall is calculated to consider the noise produced from all geometries and the shielding effect of the fairing. It is found that a noise reduction around 3 dB is achieved through mounting the fairing in the bogie area and the noise prediction from the permeable surface is generally higher than that from the bogie surfaces alone as all pressure fluctuation on the surfaces of the geometries are included by the permeable surface.

References

[1] D.J. Thompson. Railway noise and vibration: mechanisms, modelling and means of control. Elsevier, Oxford, UK, 2008.

[2] C. Mellet, F. Letourneaux, F. Poisson, C. Talotte. High speed train noise emission: Latest investigation of the aerodynamic/rolling noise contribution. Journal of Sound and Vibration, 2006, 293: 535-546.

[3] C. Talotte, P.E. Gautier, D.J. Thompson, C. Hanson. Identification, modelling and reduction potential of railway noise sources: a critical survey. Journal of Sound and Vibration, 2003, 267: 447-468.

[4] C.J. Baker. A review of train aerodynamics Part 1-Fundamentals. The Aeronautical Journal, 2014, 118: 201-228.

[5] C.J. Baker. A review of train aerodynamics Part 2-Applications. The Aeronautical Journal, 2014, 118: 345-382.

[6] E. Masson, N. Paradot, E. Allain. The numerical prediction of the aerodynamic noise of the TGV POS high-speed train power. Proceedings of the 10th International Workshop on Railway Noise, Nagahama, Japan, 2010: 457-464.
[7] M. Meskine, F. Pérot, M.S. Kim, D. M. Freed, S. Senthooran, Z. Sugiyama, F. Polidoro, S. Gautier. Community noise prediction of digital high speed train using LBM. AIAA Paper 2013-2015, 19th AIAA/CEAS Aeroacoustics Conference, Berlin, Germany, 2013.
[8] P.R. Spalart, S. Deck, M.L. Shur, K.D. Squires, M.Kh. Strelets, A.K. Travin. A new version of detached-eddy simulation, resistant to ambiguous grid densities. Theoretical and Computational Fluid Dynamics, 2006, 20: 181-195.
[9] J.E. Ffowcs-Williams, D.L. Hawkings. Sound radiation from turbulence and surfaces in arbitrary motion. Philosophical Transactions of the Royal Society of London, 1969, 342: 264-321.
[10] J.Y. Zhu, Z.W. Hu, D.J. Thompson. Analysis of aerodynamic and aeroacoustic behaviour of a simplified high-speed train bogie. Proceedings of the 11th International Workshop on Railway Noise, Uddevalla, Sweden, 2013.